

Supporting Information

Two-Step Adsorption of PtCl_6^{2-} Complexes at a Charged Langmuir Monolayer: Role of Hydration and Ion Correlations

Ahmet Uysal,^{1,*} William Rock,¹ Baofu Qiao,¹ Wei Bu,² and Binhua Lin²

¹Chemical Sciences and Engineering Division, Argonne National Laboratory, Argonne IL 60439

²Center for Advanced Radiation Sources, The University of Chicago, Chicago IL 60637

a-XR Data Fitting

The x-ray reflectivity for a known electron density profile (EDP) is calculated by

$$R(q) = R_F \left| \frac{1}{\Delta\rho} \int \frac{d\rho(z)}{dz} e^{-iz\sqrt{q(q^2 - q_c^2)^{\frac{1}{2}}}} dz \right|^2$$

Here R_F is the Fresnel reflectivity, i.e. the ideal reflection from an interface with zero roughness; q_c is the critical angle and $\Delta\rho$ is the electron density change through the interface.¹⁻² To determine an unknown EDP from a known $R(q)$, we model the interface with constant density slabs with error function interfaces:

$$\rho(z) = \rho_0 + \sum_{i=0}^n \frac{\rho_{i+1} - \rho_i}{2} \left[1 + \operatorname{erf}\left(\frac{z - z_i}{\sqrt{2}\sigma_i}\right) \right]$$

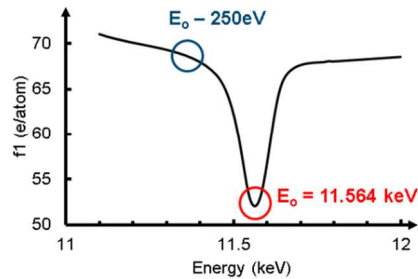
Here ρ_i and σ_i are the electron density and the roughness of i^{th} slab, respectively. We assign one layer to the head group of DPTAP and the adsorbed ions, and another layer to the tail group. Our fits determine the length (L), electron density (ρ) and interfacial roughness (σ) of the each layer (Table S1). Data from on-edge ($E_o=11.564$ keV) and off-edge (E_o-250 eV=11.314 eV) measurements at the same bulk concentration are simultaneously fit with all parameters linked except the ρ and σ in the headgroup-ion region; all other parameters will not be affected by a change in the effective number of electrons scattered by Pt. The thickness of the headgroup is fixed to 4 Å. All other parameters are allowed the float within reasonable limits.

Table S1. X-ray fitting parameters for the data sets shown in Figure 2a.^a

Bulk Concentration and x-ray Energy	σ_{subphase} (Å)	ρ_{head} ($\text{e}^-/\text{Å}^3$)	$\rho_{\text{head(im)}}$ ($\text{e}^-/\text{Å}^3$)	L_{head} (Å)	σ_{head} (Å)	ρ_{tail} ($\text{e}^-/\text{Å}^3$)	L_{tail} (Å)	σ_{tail} (Å)
5 μm E_0 -250eV	2.58	0.55	0	4*	3.78	0.33	15.68	2.47
5 μm E_0	2.49	0.54	0					
50 μm E_0 -250eV	2.28	0.61	5.68E-04	4*	3.2	0.33	16.51	2.69
50 μm E_0	2.22	0.60	5.68E-04					
1 mM E_0 -250eV	3.11	0.72	3.90E-03	4*	2.67	0.33	17.8	2.63
1 mM E_0	3.22	0.70	4.97E-03					
20 mM E_0 -250eV	3.68	0.79	1.49E-01	4*	2.74	0.33	18.51	2.66
20 mM E_0	3.68	0.74	1.76E-01					

^a The EDPs plotted in Figure 2b are based on these parameters. σ , ρ , and L represent the interfacial roughness, electron density, and thickness for each layer. The imaginary electron density ($\rho_{\text{head(im)}}$) is used for the absorption and only becomes non-zero at high Pt concentrations in the Stern layer. The absorption for other parts of the system is negligible. The subphase electron density is $0.354 \text{ e}^-/\text{Å}^3$ for all samples. *The thickness of the headgroups are fixed.

The difference between the on-edge and the off-edge measurements are caused by the number of effective electrons in Pt ions (Figure S1).³ Therefore the difference can be used to determine the elemental EDP for Pt ions (Figure 2b inset of the main text). We can calculate the area under these curves to determine the area per Pt, considering that $\sim 16 \text{ e}^-$ corresponds to 1 Pt ion. (Figure 4, main text).

**Figure S1.** Effective number of electrons of Pt ions around the L_3 absorption edge. The blue and the red circles show the energies at which the a-XR measurements were done.

DPTAP Tilt Angle Calculations

The two dimensional geometry of Langmuir monolayers limit the possible GID patterns significantly. The observation of one in-plane and one out-of-plane peak is, therefore, a clear signature of nearest neighbor (NN) tilt in a distorted hexagonal packing.⁴ In this GID pattern, out-of-plane peak is double degenerate and the in-plane peak is non-degenerate. The concentration dependent peak positions, which are listed in Table S2, are determined by fitting the peaks with a Lorentzian in the q_{xy} direction and with a Gaussian in the q_z direction. These peak positions can be used to determine the tilt angle of the tail groups from the surface normal:

$$\tan\theta = \frac{q_{dz}}{\sqrt{q_{dxy}^2 - \frac{q_{nxy}^2}{4}}}$$

where q_{dz} and q_{dxy} are the out-of-plane and in-plane peak positions for the degenerate peak, and q_{nxy} is the in-plane peak position of the non-degenerate peak.

Table S2. GID peak positions and calculated tilt angles.

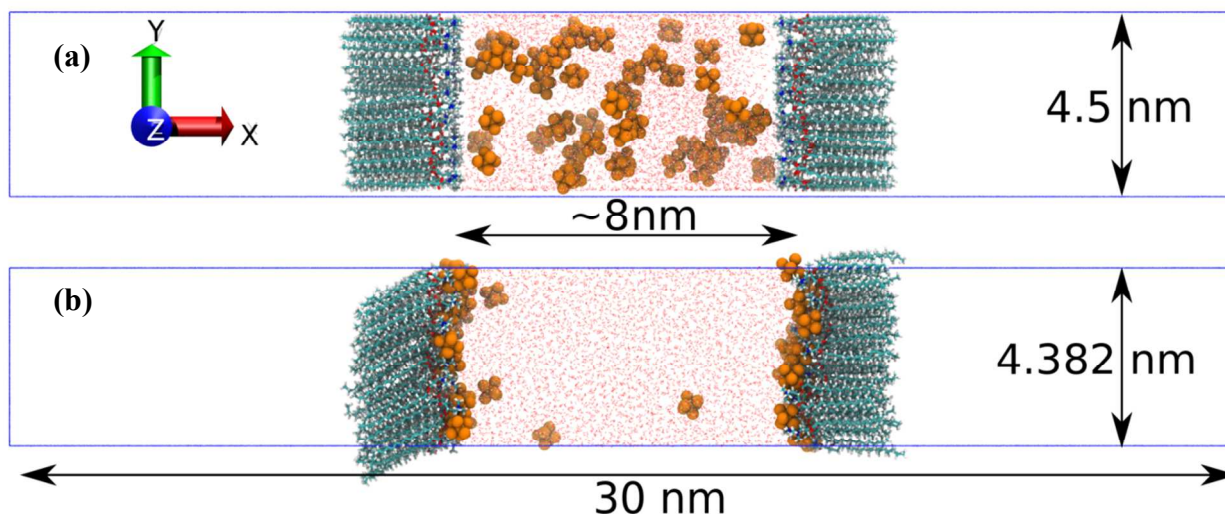
Bulk [PtCl ₆ ²⁻] (mM)	q_{dxy} (Å ⁻¹)	q_{nxy} (Å ⁻¹)	q_{dz} (Å ⁻¹)	Tilt Angle (°)
0.005	1.308	1.443	0.846	37.8
0.05	1.308	1.443	0.834	37.4
1	1.322	1.450	0.807	36.1
20	1.333	1.456	0.750	33.9

Atomistic MD Simulations

Classical MD simulations were performed using the GROMACS package (version 4.5.5).⁵ The CHARMM 36 force field⁶ was employed, which has been implemented under the GROMACS package.⁷ The force field parameters of the PtCl₆²⁻ have been reported by Lienke et al. in 2001,⁸ which were developed in the framework of the CHARMM force field. Note that the same groups reported a new version of their force field in 2011.⁹ Our simulations showed that these two sets of force fields provided quantitatively similar results regarding the surface activity of the two kinds of metalates investigated.

The CHARMM TIP3P water model was employed as in Ref. [8]. The water structure was constrained using the SETTLE algorithm.¹⁰ The force field parameters of H₃O⁺ reported by Sagnella and Voth¹¹ were employed. Given the fact that no van der Waals force field parameters for Li⁺ ions were reported for the CHARMM force field, the corresponding parameters from the AMBER force field,¹² which uses the same combination rule (Lorentz–Berthelot rule¹³⁻¹⁴) as the CHARMM force field for the non-bonded Lennard-Jones 12-6 and Coulomb interactions, were employed instead. All the other parameters were from the original CHARMM 36 force field.

The initial structure were built using the package Packmol.¹⁵ The lengths of the simulation box were $4.5 \times 4.5 \times 30 \text{ nm}^3$ in X×Y×Z dimensions. After the equilibration (see below for the details), a fixed lateral area $4.382 \times 4.382 \text{ nm}^2$ was selected to meet the experimental area per lipid of around 0.48 nm^2 per DPTAP molecule. All the molecules, except DPTAP, were initially randomly distributed inside the water region of roughly $4.5 \times 4.5 \times 8 \text{ nm}^3$. The DPTAP molecules were



located at the upper and the lower boundary of the water region with the hydrophilic headgroups extending inwards. The large vacuum region was included to mimic the experimental water/air biphasic condition (Figure S2).

Figure S2. Snapshot of the (a) initial and (b) final structures of the $0.5 \text{ M PtCl}_6^{2-}$ aqueous solution in the water/air system. The PtCl_6^{2-} ions are highlighted in orange. The lateral area of $4.5 \times 4.5 \text{ nm}^2$ was initially employed for the convenience of the system preparation using Packmol, which was changed to be $4.382 \times 4.382 \text{ nm}^2$ after the equilibration to meet the desired area per DPTAP of around 0.48 nm^2 (Figure 5b). Blue solid lines denote the simulation box boundary.

Due to the finite size effect in the MD simulations, it can be reasonably predicted that because of the adsorption at the water/DPTAP interface, the concentration of metalate in the central water region is lower than the total concentration. That is to say, the metalates will be distributed partially in the central water region, contributing to the “effective concentration” in the bulk water regime, and partially at the water/DPTAP interface regime. In this regard, we first simulated a series of aqueous solutions by varying the total concentrations of $[\text{PtCl}_6^{2-}] = 0.1, 0.2, 0.4, 0.5, 0.6, 0.7, 0.8 \text{ M}$. See the following section for the simulation equilibration process. It was found that when $[\text{PtCl}_6^{2-}] = 0.5 \text{ M}$, some metalate complexes stayed dissolved in the bulk water region dynamically, and the positive charges from the DPTAP headgroup were compensated (or slightly overcompensated) by the negative charges from the metalates. At concentrations lower than 0.5 M , all the metalates were distributed close to the water/DPTAP interface. The difference in the metalate adsorption at low concentration between the simulations and the experiments possibly indicates an underestimated hydration free energy in the simulations, which was not taken into account in the force field development.⁸ In comparison, at concentrations higher than

0.5 M, a larger amount of metalates were distributed in the central water region. Therefore, in what follows, we will focus on the systems with the total concentration of 0.5 M metalates, which is the best description of the Stern layer in the 20 mM solution in the real experiments. Orders of magnitude difference in interfacial and bulk concentrations is expected in these systems. The limitations on the simulation box size prevents us from exactly matching both conditions, and therefore we focus on the interface. A similar concern is also valid for H_3O^+ ions. Only one ion in our simulation box is enough to make the $\text{pH}=2$. However, a single ion in the simulation box cannot have a significant effect on the results. Nevertheless, we do not expect this to cause a significant issue in determining the Stern layer structure, because H_3O^+ ions are already repelled from the positively charged surface.

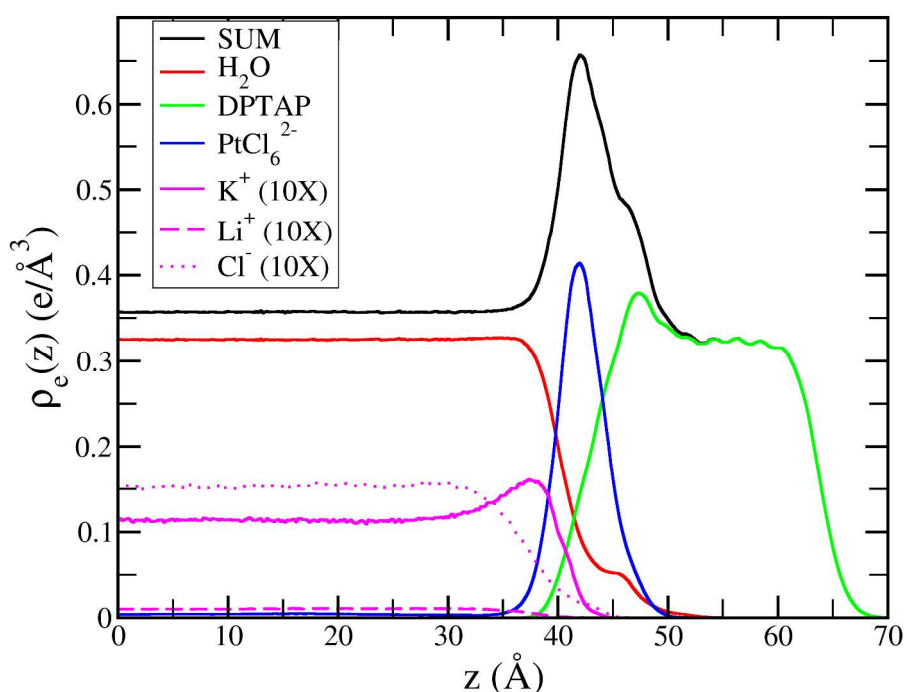
Table S2. Numbers of the Components in the Simulation of 0.5M PtCl_6^{2-}

	$[\text{PtCl}_6]^{2-} \cdot \text{K}_2^+$ ^a	$\text{Li}^+ \cdot \text{Cl}^-$ ^b	$[\text{H}_3\text{O}]^+ \cdot \text{Cl}^-$ ^c	$\text{DPTAP}^+ \cdot \text{Cl}^-$ ^d	H_2O
0.5M PtCl_6^{2-}	50	50	1	80	5200

- K^+ are counterions of metalates
- $[\text{Li}^+ \cdot \text{Cl}^-] = 0.5 \text{ M}$.
- $[\text{H}_3\text{O}^+ \cdot \text{Cl}^-] = 0.01 \text{ M}$ ($\text{pH} = 2$)
- Lateral area per DPTAP is 0.48 nm^2 .

As aforementioned, all the molecules were initially randomly located in the water regime, with the DPTAP capped at the upper and lower boundaries in the Z-dimension (Figure S2a). The energy minimization of the initial structure was performed using the steepest descent algorithm. Each of the systems was subsequently equilibrated using semi-isotropic pressure coupling ($P_{XY} = P_Z = 1 \text{ bar}$). The other simulation parameters were the same as those employed in the production simulations below. The equilibration simulation ran for a duration of 10 ns.

The lateral area of $4.382 \times 4.382 \text{ nm}^2$ was then applied to reach the desired area per DPTAP of 0.48 nm^2 . The following production simulation ran for 220 ns, with the simulation frames from the last 200 ns saved using a saving frequency of 10 ps per frame for the subsequent data analysis. In the production simulations, the NTV ensemble (constant number of particles, temperature, and volume) was used. The reference temperature was 298 K, with waters and the other molecules separately coupled using the velocity rescaling algorithm (time constant 0.1 ps). Three-dimensional periodic boundary conditions were employed. Neighbor searching was done up to a cutoff distance of 1.2 nm. The short-range Coulomb interactions were calculated up to this cutoff distance with the long-range Coulomb interactions calculated using the smooth Particle Mesh Ewald (PME) method with a grid real spacing of 0.12 nm and cubic interpolation.¹⁶⁻¹⁷ The Lennard-Jones 12-6 potential was employed for the van der Waals interactions, which was calculated up to the cutoff distance of 1.2 nm, with the long-range



dispersion correction for the energy and pressure applied. A simulation integration time step of 2 fs was employed with all the hydrogen-involved covalent bond lengths constrained using the LINCS algorithm.¹⁸

Figure S3. Electron density of the different components in the system with 0.5 M PtCl_6^{2-} . The reference ($z = 0$) is based on the geometric center of all water molecules in the simulation box.

SI References

1. Uysal, A.; Chu, M.; Stripe, B.; Timalsina, A.; Chattopadhyay, S.; Schlepütz, C. M.; Marks, T. J.; Dutta, P. What x rays can tell us about the interfacial profile of water near hydrophobic surfaces. *Physical Review B* **2013**, *88* (3), 035431.

2. Pershan, P. S.; Schlossman, M. *Liquid Surfaces and Interfaces: Synchrotron X-ray Methods*. Cambridge University Press: 2012.
3. Henke, B. L.; Gullikson, E. M.; Davis, J. C. X-ray interactions: photoabsorption, scattering, transmission, and reflection at $E= 50\text{-}30,000$ eV, $Z= 1\text{-}92$. *Atomic data and nuclear data tables* **1993**, *54* (2), 181-342.
4. Kaganer, V. M.; Mohwald, H.; Dutta, P. Structure and phase transitions in Langmuir monolayers. *Reviews of Modern Physics* **1999**, *71* (3), 779-819.
5. Hess, B.; Kutzner, C.; van der Spoel, D.; Lindahl, E. GROMACS 4: Algorithms for Highly Efficient, Load-Balanced, and Scalable Molecular Simulation. *J. Chem. Theory Comput.* **2008**, *4*, 435-447.
6. Best, R. B.; Zhu, X.; Shim, J.; Lopes, P. E.; Mittal, J.; Feig, M.; Mackerell, A. D., Jr. Optimization of the additive CHARMM all-atom protein force field targeting improved sampling of the backbone phi, psi and side-chain chi(1) and chi(2) dihedral angles. *J. Chem. Theory Comput.* **2012**, *8* (9), 3257-3273.
7. Bjelkmar, P.; Larsson, P.; Cuendet, M. A.; Hess, B.; Lindahl, E. Implementation of the CHARMM Force Field in GROMACS: Analysis of Protein Stability Effects from Correction Maps, Virtual Interaction Sites, and Water Models. *J. Chem. Theory Comput.* **2010**, *6* (2), 459-66.
8. Lienke, A.; Klatt, G.; Robinson, D. J.; Koch, K. R.; Naidoo, K. J. Modeling platinum group metal complexes in aqueous solution. *Inorg. Chem.* **2001**, *40* (10), 2352-7.
9. Matthews, R. P.; Venter, G. A.; Naidoo, K. J. Using Solvent Binding and Dielectric Friction To Interpret the Hydration Behavior of Complex Anions. *J. Phys. Chem. B* **2011**, *115* (5), 1045-1055.
10. Miyamoto, S.; Kollman, P. A. SETTLE: An Analytical Version of the SHAKE and RATTLE Algorithm for Rigid Water Models. *J. Comput. Chem.* **1992**, *13*, 952-962.
11. Sagnella, D. E.; Voth, G. A. Structure and dynamics of hydronium in the ion channel gramicidin A. *Biophys. J.* **1996**, *70* (5), 2043-2051.
12. Case, D. A.; Cheatham, T. E., 3rd; Darden, T.; Gohlke, H.; Luo, R.; Merz, K. M., Jr.; Onufriev, A.; Simmerling, C.; Wang, B.; Woods, R. J. The Amber biomolecular simulation programs. *J. Comput. Chem.* **2005**, *26*, 1668-88.
13. Lorentz, H. A. Ueber die Anwendung des Satzes vom Virial in der kinetischen Theorie der Gase. *Annalen der Physik* **1881**, *248* (1), 127-136.
14. Berthelot, D. Sur le mélange des gaz. *C. R. Hebd. Seances Acad. Sci.* **1898**, *126*, 1703-1855.
15. Martínez, L.; Andrade, R.; Birgin, E. G.; Martínez, J. M. PACKMOL: A Package for Building Initial Configurations for Molecular Dynamics Simulations. *J. Comput. Chem.* **2009**, *30*, 2157-2164.
16. Darden, T.; York, D.; Pedersen, L. Particle Mesh Ewald: An $N \cdot \log(N)$ Method for Ewald Sums in Large Systems. *J. Chem. Phys.* **1993**, *98*, 10089-92.
17. Essmann, U.; Perera, L.; Berkowitz, M. L.; Darden, T.; Lee, H.; Pedersen, L. A Smooth Particle Mesh Ewald Method. *J. Chem. Phys.* **1995**, *103*, 8577-93.
18. Hess, B. P-LINCS: A Parallel Linear Constraint Solver for Molecular Simulation. *J. Chem. Theory Comput.* **2008**, *4*, 116-122.